Submesoscale Instability in the Straits of Florida

LAURENT M. CHÉRUBIN,[a] NICOLAS LE PAIH,[b] AND XAVIER CARTON[c]

[a] *Harbor Branch Oceanographic Institute, Florida Atlantic University, Fort Pierce, Florida*
[b] *Alfred-Wegener-Institute Helmholtz Centre for Polar and Marine Research, Bremerhaven, Germany*
[c] *Département de Physique, IUEM/LOPS UFR Sciences, Plouzané, France*

(Manuscript received 22 November 2020, in final form 27 April 2021)

ABSTRACT: The Florida Current (FC) flows in the Straits of Florida (SoF) and connects the Loop Current in the Gulf of Mexico to the Gulf Stream (GS) in the western Atlantic Ocean. Its journey through the SoF is at time characterized by the formation and presence of mesoscale but mostly submesoscale frontal eddies on the cyclonic side of the current. The formation of those frontal eddies was investigated in a very high-resolution two-way nested simulation using the Regional Oceanic Modeling System (ROMS). Frontal eddies were either locally formed or originated from outside the SoF. The northern front of the incoming eddies was susceptible to superinertial shear instability over the shelf slope when the eddies were pushed up against the slope by the FC. Otherwise, incoming eddies could be advected, relatively unaffected by the current, when in the southern part of the straits. In the absence of incoming eddies, submesoscale eddies were locally formed by the roll-up of superinertial barotropically unstable vorticity filaments when the FC was pushed up against the shelf slope. The vorticity filaments were intensified by the friction-induced bottom-layer vorticity flux as previously demonstrated by Gula et al. in the GS. When the FC retreated farther south, negative-vorticity west Florida shelf waters overflowed into the SOF and led to the formation of submesoscale eddies by baroclinic instability. The instability regimes, that is, the submesoscale frontal eddies formation, appear to be controlled by the lateral ''sloshing'' of the FC in the SoF.

KEYWORDS: Ocean; North America; Boundary currents; Instability; Regional models

1. Introduction

In the last two decades, submesoscale coherent vortices (SCVs) have been the subject of a significant amount of research (McWilliams 2016). Indeed, with the advancement of remote sensing observations of ocean color and ocean currents, Lagrangian measurements and high-resolution numerical simulations, the ubiquity of SCVs has become evident. These coherent flow structures have a significant role in the energy dissipation in the world's oceans to which they provide a unique pathway (McWilliams 2016). They are characterized by their small scale (0.1–10 km in the horizontal) less than the local first baroclinic Rossby radius (R_d), their vigorous circulation (Rossby number Ro > 1), which make them unbalanced, and their short life span although some SCVs in the ocean interior can last several years.

SCVs appear to form as the spontaneous expression of the dynamical unbalance in oceanic system, which is broken by the development of small-scale perturbations. They are known as mixed layer instability (MLI; Boccaletti et al. 2007), which is a baroclinic instability in a weakly stratified layer, which forms SCVs known as mixed layer eddies (MLEs). Strain induced frontogenesis associated with mesoscale eddy circulation or currents lead to the formation of dense filaments that becomes unstable and form submesoscale eddies (Lapeyre et al. 2006; Capet et al. 2008; Manucharyan and Timmermans 2013; Zhong and Bracco 2013; Gula et al. 2014). While frontogenesis can occur independently from MLI, the two processes often accompany each other with secondary frontogenesis arising on the edges of MLEs.

SCVs are also formed as the result of the energy dissipation process of boundary currents or mesoscale eddies when impinging against the bathymetry (Evans et al. 2020). Such process was first described by Molemaker et al. (2015), who demonstrated that currents in a boundary layer along a slope do generate a horizontal shear, which is a source of vertical vorticity of the flow. Using this argument, Gula et al. (2015b) demonstrated the role of this mechanism in the formation of frontal submesoscale eddies on the cyclonic flank of the Gulf Stream (GS). These cyclonic eddies were formed by the destabilization of vorticity filaments created by the friction of the boundary current on the shelf slope. The filaments became unstable after separation of the current from the coast. In another region of the world's ocean, the Omani Coastal Current is a boundary current that flows northward along the southern coast of Oman during the summer monsoon. A similar mechanism appears to sustain the formation of submesoscale frontal eddies, although the source of the strong shear was not shown. But they are generated by the instability of the horizontal shear that cancels the current at the coast as shown by Morvan and Carton (2020). Submesoscale frontal eddies are also observed in the frontal region of the Agulhas Current as revealed by buoyancy gliders surveys in Krug et al. (2017). Eddies are observed in a region where the current velocity core flows above the shelf as is the case for the GS in the region studied by Gula et al. (2015b). In a high-resolution simulation of the Agulhas Current, Tedesco et al. (2019) showed the formation of a

Supplemental information related to this paper is available at the Journals Online website: https://doi.org/10.1175/JPO-D-20-0283.s1.

Corresponding author: Laurent Chérubin, lcherubin@fau.edu

DOI: 10.1175/JPO-D-20-0283.1

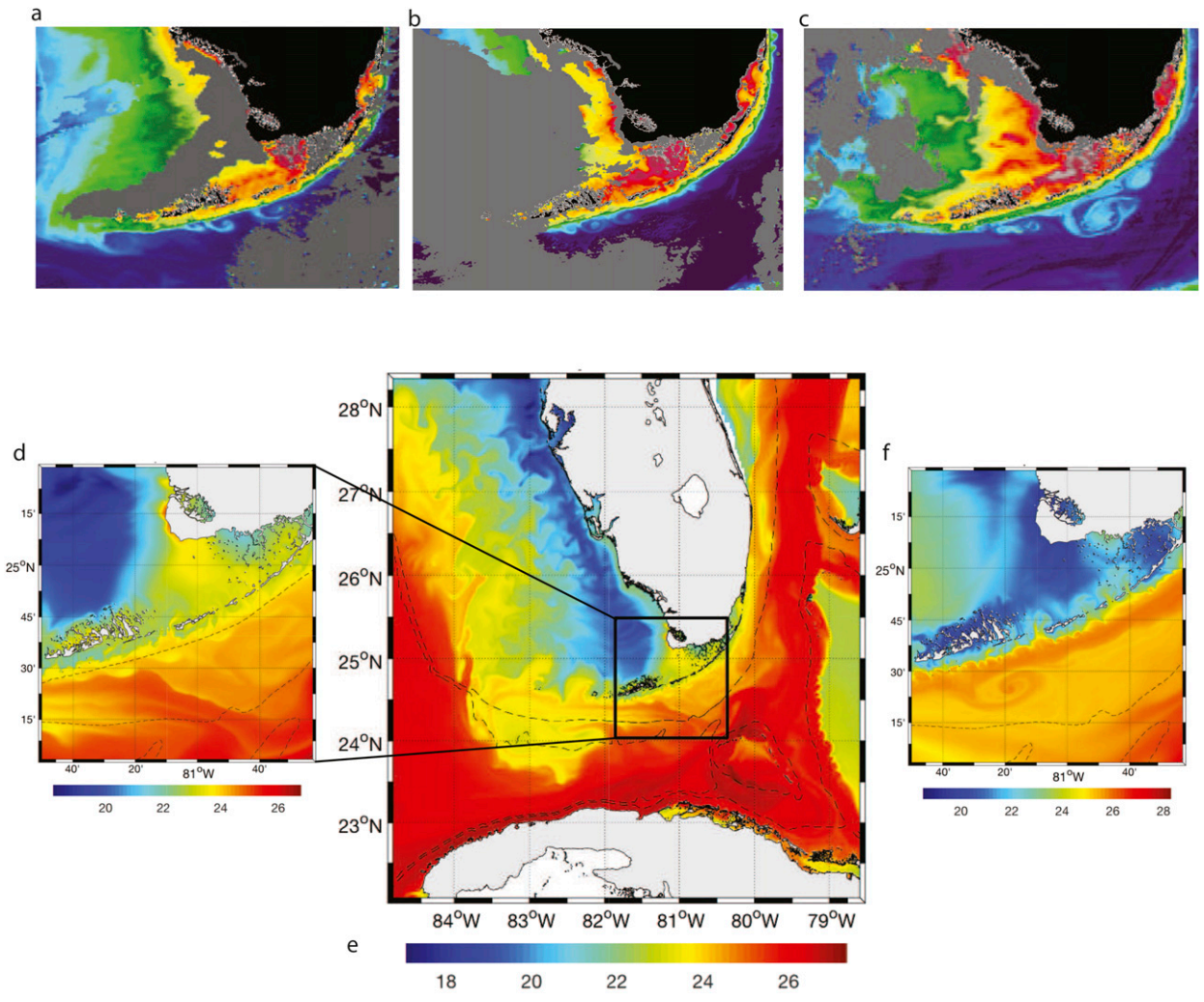

FIG. 1. (a)–(c) 3-day average Chl-a images of submesoscale frontal eddies in the southern Straits of Florida. Chl-a was estimated from MODIS measurements and images provided by Optical Oceanography Observatory at University of South Florida. The images cover 24°–26°N, 83°–80°W. (d) FB-ROMS nested model SST showing submesoscale frontal eddies SE6 at model time t = 371 days. (e) FB-ROMS SST parent and child domain on model time t = 317 days. (f) FB-ROMS model SST showing submesoscale eddy SE3 at model time t = 335 days. Note the similarity between model and observations.

vortex street by barotropic instability of the sheared frontal region of the current. Such vortex streets are also observed in the southern part of the Straits of Florida (SoF; Fig. 1) where the core of the Florida Current (FC) flows against the shelf slope. The destabilization of the topographically induced frontal cyclonic shear of the FC is the focus of the study herein.

The FC, which is confined within the SoF, connects the Loop Current in the eastern Gulf of Mexico to the south with the GS to the north in the South Atlantic Bight. The axis of the FC core is located in the northern SoF, 5–10 km from the shelf break, east of Miami and Palm Beach, Florida (FL) (Molinari and Leaman 1987; Beal et al. 2008), and 10–15 km south of Key West, FL, in the southern SoF. The FC follows the topography where the shelf progressively gets narrower from the Florida Keys to Ft. Lauderdale, FL. Generally, the flow is toward the east before veering north around 81°W longitude. The FC transport exhibits a seasonal cycle characterized by a maximum in May–July and a minimum in January. However, most of the variability is observed on time scales of 4–20 days. The variability has been related to changes in along-stream wind stress, continental shelf waves, meanders modes, and frontal eddies (Brooks and Niiler 1977; Johns and Schott 1987; Lee and Williams 1988; Lee et al. 1991; Fiechter and Mooers 2003).

The flow over the outer shelf is frequently affected by the meanders and perturbations of the highly sheared FC's northern and western edges. FC perturbations vary from slow-moving mesoscale gyres (Lee and Williams 1988) to faster-moving, submesoscale eddies (Lee 1975). Such fluctuations typically dissipate over the shelf break and are not usually detected in current meter observations over the inner shelf (Lee 1986). Surface velocity measurements from the Ocean Surface Current Radar (OSCR) in high-resolution

mode (Shay et al. 2000, 2002; Archer et al. 2015) suggest that the FC is an oceanic feature characterized by large horizontal shears on its cyclonic side, relative vorticities up to 11 times the local Coriolis parameter (f) and strong topographical constraints as found by Peters et al. (2002).

The FC frontal eddies encompass a radius of 2–30 km (Shay et al. 1998; Richardson et al. 2009; Kourafalou and Kang 2012), which is often smaller than the deformation radius of 10–30 km (Shay et al. 2007). They are short-lived (1–2 weeks), swift because they travel with the flow, and appear trapped against the Florida shelf slope. Unlike frontal eddies observed in the northern SoF (Lee et al. 1991; Fiechter and Mooers 2003; Gula et al. 2015a,b), few Florida Keys Reef Tract (FKRT) eddies have a cold sea surface temperature signature associated with the cyclonic circulation-driven upwelling (Kourafalou and Kang 2012; Richardson et al. 2009). In fact, the passage of frontal eddies in the lower Keys in June and July shows a temperature increase in surface waters (Sponaugle et al. 2005) as warmer waters from the west Florida shelf are entrained at the surface by the FC (Kourafalou and Kang 2012). This is consistent with the warm-water anomaly observed by Richardson et al. (2009). At the bottom, the passage signature of the frontal eddies can also include a cold-water bore generated by the impingement of the eddy on the shelf slope (Sponaugle et al. 2005; Davis et al. 2008).

Several hypotheses have been put forth to explain the formation of submesoscale eddies: (i) growing barotropic instabilities (meanders) (Lee and Mayer 1977); (ii) part of the final growth stage of baroclinically unstable meanders (Lee et al. 1992); (iii) abrupt changes in wind direction and stress over the shelf (Shay et al. 1998); (iv) associated with the cyclonic side of the FC meanders along the Florida shelf (Fiechter and Mooers 2003); (v) decay of mesoscale eddies (Lee et al. 1995; Sponaugle et al. 2005). The most recent work by Gula et al. (2015b) identified the instability of potential vorticity (PV) filaments as a dominant mechanism for the formation of small frontal eddies in the northern SoF. Using a high-resolution simulation realized with the Regional Oceanic Modeling System (ROMS), Gula et al. (2015b) analyzed the role of bottom induced vorticity on the formation of large, positive, relative vorticity (RV) filaments (up to 3–4f) on the cyclonic side of the GS. The bottom drag against the slope amplifies the cyclonic shear according to the mechanism described by Molemaker et al. (2015). The sloped turbulent bottom boundary layer also provides a source of PV as shown by Gula et al. (2015b). The topographically intensified positive-vorticity filament in the model was found to be about 2–3 km wide and became unstable once the FC separated from the coast near West Palm Beach, FL. The filament rolled up into a street of submesoscale vortices, known as ''spinoff eddies.'' This mechanism was identified by Rayleigh (1880) who showed that an isolated two-dimensional vorticity filament is always unstable and rolls up into discrete vortices.

Small-scale frontal eddies in the SoF, on the cyclonic side of the FC are frequently observed and present a wide variety of numbers, shapes, and sizes that would suggest different origins and formation mechanisms. As shown by the previous literature (Kourafalou and Kang 2012), the larger (mesoscale) eddies have a remote origin, but a closer look at the smaller eddies show that they originated in the SoF (Fig. 1) as confirmed by Zhang et al. (2019).

To investigate the formation of these eddies, we used a 500-m resolution simulation of the circulation along the FKRT (Figs. 1d–f). This simulation was two-way nested in a larger South Florida simulation described in Criales et al. (2015), both realized with ROMS. The visual analysis of the nested model revealed the formation and the presence of various types of mesoscale and submesoscale frontal eddies with striking resemblance to observed eddies in MODIS/MERIS Chl-a images in the southern SoF (see, e.g., eddies in Figs. 1a,d,e and 1c,f). We therefore investigated the mechanism of formation and the origin of the small eddies based on energetics and PV fluxes. We show that vorticity filaments are also unstable within the Straits, while the current is in contact with the upper slope. In addition, we show that the west Florida shelf (WFS) is a source of negative-vorticity waters that sustains the frontal instabilities of the FC in the southern SoF. In section 2 we present the model setup, in section 3 we describe the eddy regimes. The eddies mechanisms of formation are analyzed in section 4 and along with the bottom vorticity generation process in section 5. Concluding remarks are given in section 6.

2. Model setup

The numerical simulation used in this study was a realization of the ROMS two-way nested South Florida simulation. The full two-way nesting allows the interaction of multiscale dynamics across the nest boundaries (Debreu et al. 2012). While the parent grid, with a 1.5-km horizontal resolution encompassed the South Florida region, from the Gulf of Mexico to the Atlantic Ocean, a 500-m nest was centered on Florida Bay and encompassed the northern part of the southern SoF (Fig. 1). This nest is called hereafter the FB-ROMS. The location of the nest within the parent grid is such that incoming mesoscale eddies from the parent grid enter the nested grid. Therefore, the dynamics of the incoming eddies could be affected by the change in grid resolution. This particular problem was investigated by Debreu et al. (2012) with the case study of a baroclinic vortex on a β-plane crossing between the coarse- and high-resolution grids. With two-way nesting, the parent grid solution is updated from the child allowing smooth, continuous interfacing between grid levels. However, as opposed to one-way nesting, the updated parent solution has no intrinsic value in the refinement area and cannot be used for estimating resolution sensitivity. Using a reference solution computed at high resolution, Debreu et al. (2012) showed continuity of fine and coarse solutions at the grids' interface; dynamical integrity of the solutions in the refinement area (as a result of better interface transparency); and improvements outside the refinement area. These results also demonstrated the superiority of the refinement area solution over a one-way nesting approach. ROMS was also used with two-way nesting enabled to study submesoscale dynamics in tropical instability waves (TIWs; Marchesiello et al. 2011). Using three nested grids, they showed that the TIW can travel through two nested interfaces without alteration of its wave properties. The finest

TABLE 1. Rossby number Ro is calculated as the mean of ζ/f at 5 m deep along a transect across the eddy. The values in parentheses indicate the maximum of ζ/f observed in the eddy.

Eddy	LSE1	SE1	LSE2	ME1	SE2	SE3	SE4	SE5	SE6	SE7	SE8
Model day count	282–292	288–296	301–306	316–325	325–329	332–340	346–357	361–363	368–375	378–382	403–408
Ro (ζ/f)	1.6 (7.0f)	1.5 (3.5f)	1.2 (3.0f)	0.77 (2.0f)	1.1 (2.5f)	1.2 (3f)	2.0 (7.5f)	1.6 (5.5f)	3.1 (6.5f)	1.8(5.5f)	2.3 (4.0f)
Minor–major axis lengths	28–56 km	18–31.5 km	25–29 km	41–74 km	6–18 km	17–34 km	10–25 km	10–27 km	12–14 km	14–30 km	22–30 km

grid exhibited the development of SVCs not generated in the coarser grid, which is also the case in our study.

The model has 25 levels on the vertical and the vertical grid spacing does not exceed 30 m in the region of strong topographic vorticity generation. The bathymetry was built from the 90-m resolution U.S. Coastal Relief Model Vol. 3 (Florida and East GoM). The use of sigma coordinates, which consist of layers that follow the bathymetry with increasing resolution toward the shallow region, is beneficial to the representation of frictional effects and bottom pressure forces and torque on the overlaying flow (Magaldi et al. 2008; Molemaker et al. 2015; Gula et al. 2015a).

The circulation of the ROMS model was forced at the surface by the National Centers for Environmental Prediction (NCEP) North American Regional Reanalysis (NARR; Mesinger et al. 2006) for the years 2003 and 2004 after a 6-month spinup in the first half of 2003. The model surface was forced by 3-hourly wind, air temperature, relative humidity, evaporation, and precipitation rates. Wind stress was calculated by the model's air–sea fluxes bulk formulation. Four-hourly net surface shortwave and longwave heat fluxes, as well as the net shortwave radiation were obtained from the NCEP–National Center for Atmospheric Research (NCAR) reanalysis (Kalnay et al. 1996). The model sea surface temperature (SST) was relaxed daily to the coarser 4-km resolution night SST from National Oceanic and Atmospheric Administration's (NOAA) Advanced Very High Resolution Radiometer (AVHRR) Pathfinder SST v5 (Casey et al. 2010). At the lateral boundaries, the parent model was forced by tides from the TPXO7 model (Egbert and Erofeeva 2002) and by the Gulf of Mexico-HYCOM (GOM-HYCOM) ocean state analysis (Zamudio and Hogan 2008; Chassignet et al. 2009).

3. Eddy regimes

In this section we describe the eddy regimes observed in the model. Eddies are either incoming eddies outside the nest domain or are formed locally. An animation of the relative vorticity field is provided in the online supplemental information. We also classify them in two categories, one associated with mesoscale eddies and the other one with submesoscale eddies. The distinction between the two types is made based on their averaged Rossby number Ro ≥ 1 (Ro ≤ 1) for submesoscale (mesoscale) eddies. The time period analyzed in this study, which spans model months September 2003 to February 2004 reveals a succession of mesoscale and submesoscale eddies, the latter being formed at time in the wake of previous eddies (Table 1).

Figure 2 shows all the eddy regimes in terms of their relative vorticity (ζ/f) captured in this sequence. The mesoscale eddy ME1 and the large submesoscale eddies LSE1 and LSE2 were advected from outside the nested model domain. All the other submesoscale eddies were formed within the nested model domain along the FKRT. The size of most submesoscale eddies in our simulation fell within the size range distribution identified by Zhang et al. (2019), who showed a normal distribution of size centered around 15 km. As shown in Table 1, most eddies were elliptical and strongly deformed by the current's strain field. In all cases, submesoscale eddies were formed in less than a day. Figure 2 also reveals the ubiquity of vorticity

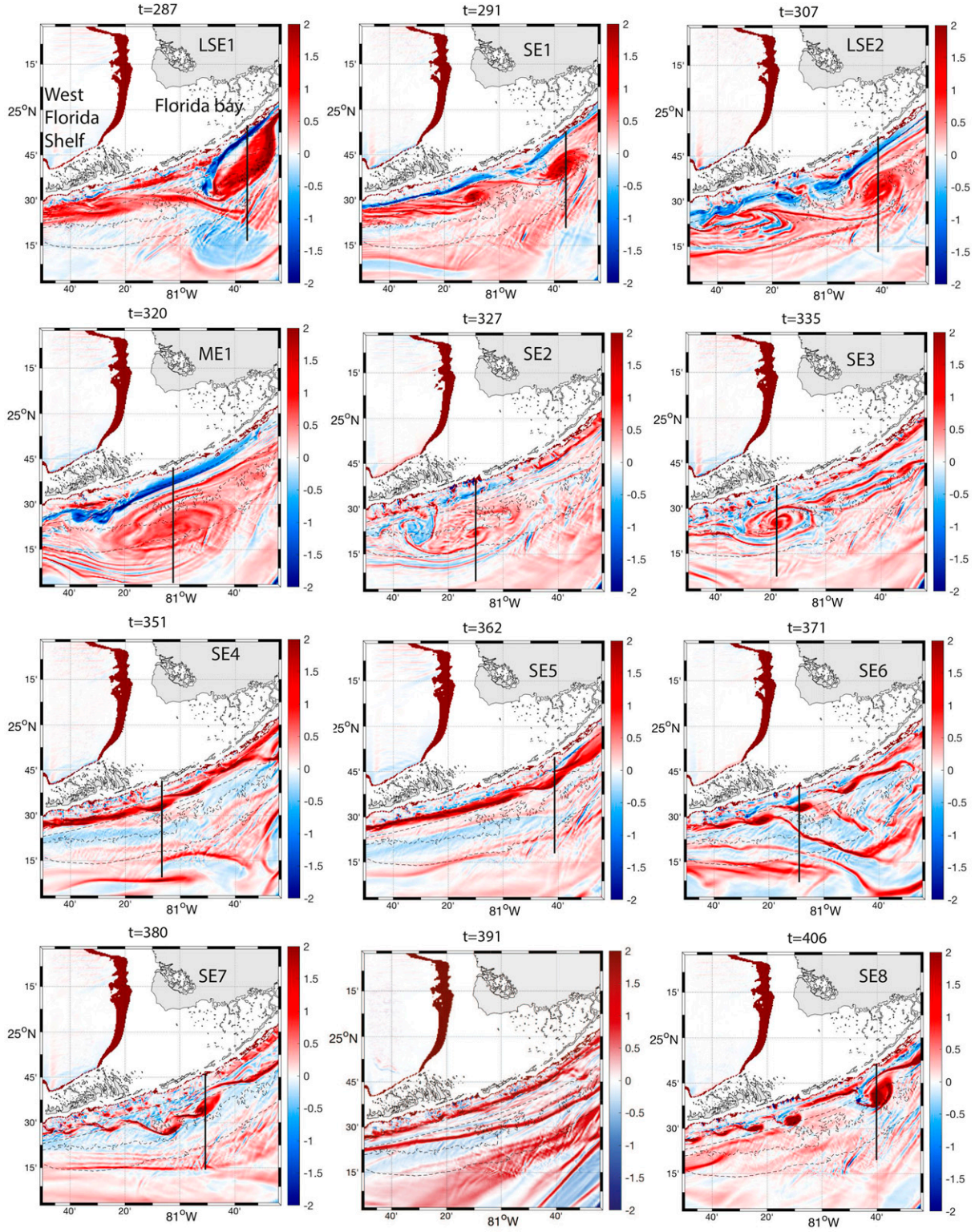

FIG. 2. Sequence of relative vorticity field (ζ/f) calculated at −5 m associated with each of the eddies described in Table 1. The time t in model days is indicated above each panel. The vertical line indicates the location of the cross sections in Fig. 3.

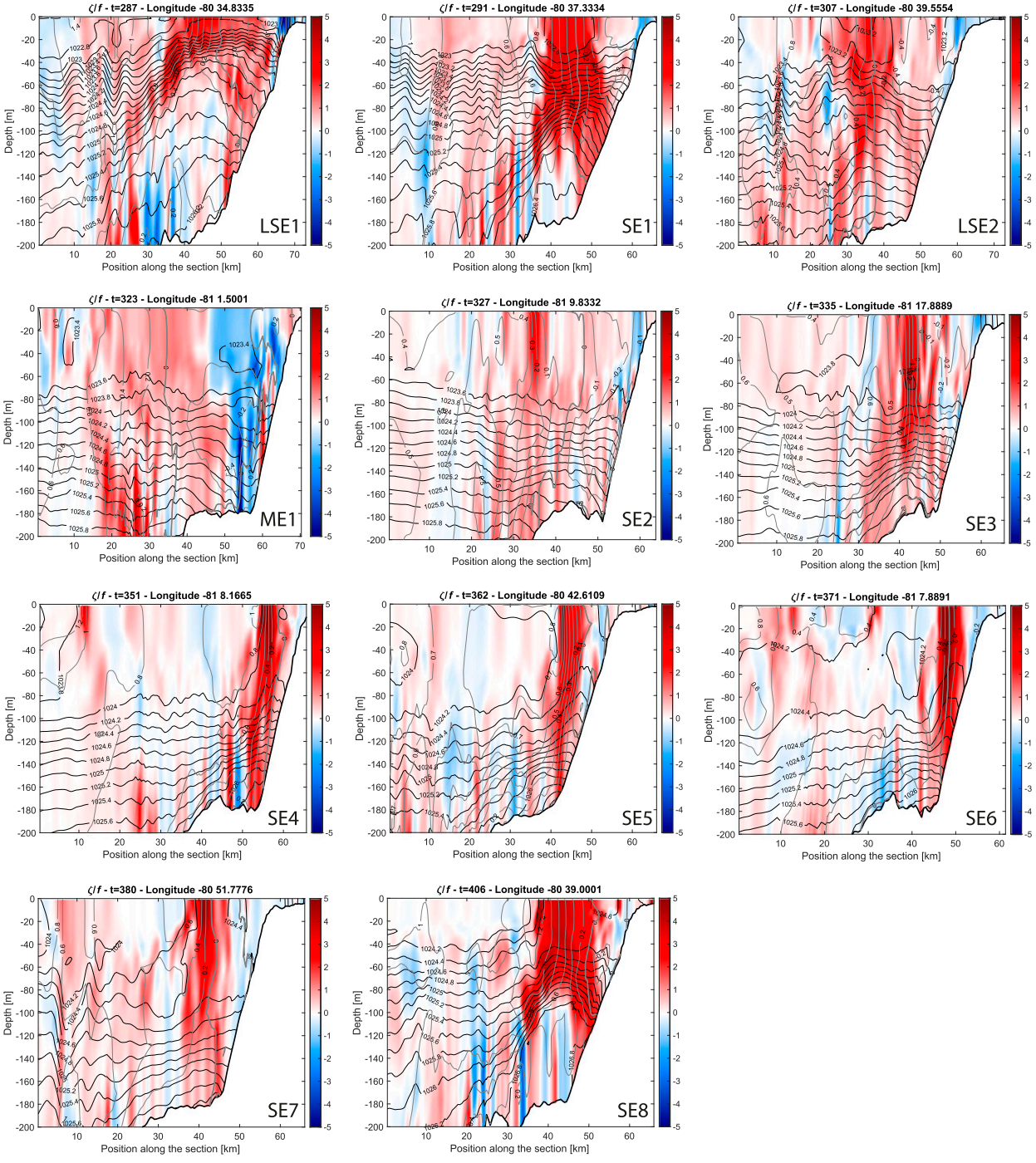

FIG. 3. Sequence of relative vorticity field (ζ/f) cross section for each eddy identified in Table 1. The time t in model days is indicated above each panel. Black contours show the density in kg m^{-3}. The density interval is 0.2 kg m^{-3}. Gray contours show the zonal velocity in m s^{-1}. Gray thick line shows the zero velocity contour. The velocity interval is 0.1 m s^{-1}.

filaments associated with the formation of the frontal eddies. Most filaments that roll up into vortices are associated with the 50-m isobath from the surface but we will show in the next section that in some of the cases they are reaching the bathymetry between 50 and 150 m.

The respective mesoscale and submesocale eddies vertical structure can be assessed from the panels shown in Fig. 3. Most eddies are associated with a strong upwelling within their core, except for a few exceptions. SE1 shows no signs of surface upwelling. Instead, isopycnals converge at about 70 m and

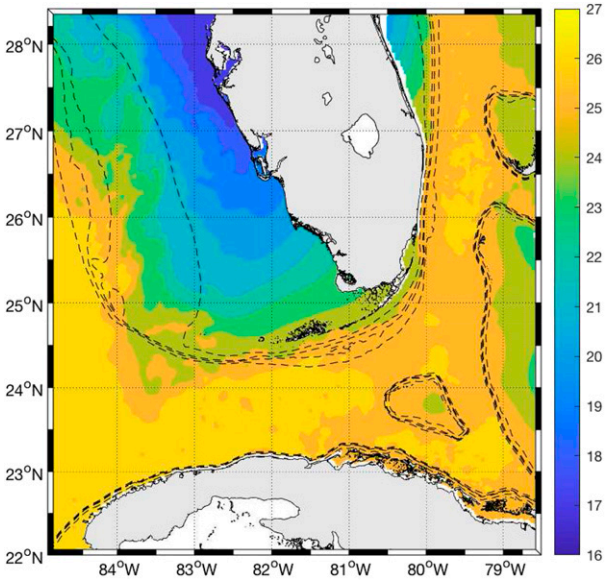

FIG. 4. Group for High Resolution Sea Surface Temperature (GHRSST) observed 1 Jan 2004.

suggest that this eddy was subsurface intensified. It appears that most eddies generated in close proximity to the shelf slope exhibit larger isopycnal rise than other eddies farther from the slope. SE1 and SE2 for example are not associated with isopycnal rise near the surface, nor is SE3, although their average relative vorticity at 5 m largely exceeds f as shown in Table 1. In the next section we analyze the eddy formation processes for all eddies in Table 1. We first identify the water masses they are associated with and then we use an energetic analysis to infer the nature of the current instability that led to their formation.

4. Eddies origin, instability, and vortex formation

a. Eastern LC front incoming frontal eddies

The high resolution of this simulation enables the development of a turbulent LC eastern boundary layer that seeds significant instability. A large number of eddies and filaments of various sizes are formed along the edge and entrain in this frontal region a large amount of shelf water, which is mixed with LC waters (Barth et al. 2008; Fig. 4). As shown by Fratantoni et al. (1998), these eddies migrate quickly and enter the southern SoF where they are known as the Tortugas Gyres. Kourafalou and Kang (2012) showed that they undergo strong transformation. Individual eddies can split in multiple vortices as they become elongated by the FC shear on their southern side and by friction on the shelf slope on their northern side.

In our simulation, LSE1 and LSE2 originated from the LC eastern frontal region and became elongated as they entered the southern SOF (Fig. 5). While moving through the strait, the strong shear instability on their northern front (see section 4c) led to the growth of a meander that embedded the incoming eddy into a dipole (Figs. 5d,e,h,i). ME1 also originated from the LC eastern frontal region, but did not undergo the same elongation process as the previous two. Instead it traveled through the southern strait keeping close to its incoming size although shear instability growth on its northern front was present (Fig. 6). We will show in section 6 that the fate of the incoming eddies is controlled by the latitudinal location of the FC in the southern SoF.

b. Locally formed frontal eddies

All the other eddies identified in this model time span were formed within the southern SoF. A review of their formation through the evolution of their relative vorticity ζ, shows that all the small-scale eddies were formed from the breakup and roll-up of vorticity filaments located over the shelf slope. Although we singled out one eddy in the chain (Table 1), all eddy regimes except for SE2 and SE3 consisted of an eddy chain. One eddy regime involved more than one vorticity filament as was the case for SE3 (Fig. 2). In most cases the strongest vorticity filament hovers over the 50–150-m depth range but more surface filaments farther offshore are present. They seem to contribute to the large cyclonic shear region between the FC and the shelf slope of the FKRT. We will address in section 5 the formation process of the vorticity filaments in light of the mechanism described by Gula et al. (2015b). Most eddies are formed in less than a day and traveled over four days across the nested model domain as observed for SE6 (Fig. 2) for example. The average translational speed was about 20 km day^{-1} or 0.24 m s^{-1}. The last eddy formed in the SE6 chain, remained within the domain, and was reabsorbed by the new vorticity filaments that emerged in the lee of SE6 and formed the new eddy chain that SE7 belonged to. This type of interaction suggests that the locally formed submesoscale eddies can be trapped near their region of formation rather than being advected away, adding to the complexity of the FC frontal region dynamics.

c. Instability analysis

To identify the sources of instability we followed the method proposed by Gula et al. (2014). We conducted a local eddy-mean analysis at the time of maximum amplification of the perturbation. The time of maximum amplification can be obtained from the eddy kinetic energy (EKE) time evolution shown in Fig. 7. This figure shows that the frontal instability of the incoming mesoscale eddies is associated with a peak in EKE as well as the formation of the submesoscale eddies. Because the energy conversion process was consistent throughout the growth phase of the instability, we chose to present the conversion rate at one given instant during the growth phase. We computed the kinetic energy conversion terms between the flow and its perturbation in a local frame of reference aligned with the local direction of the vorticity filament or with the along shelf direction of the eddy northern front in the case of the incoming eddies.

The local coordinates are x in the along-front and y in the cross-front direction, respectively, and the corresponding local

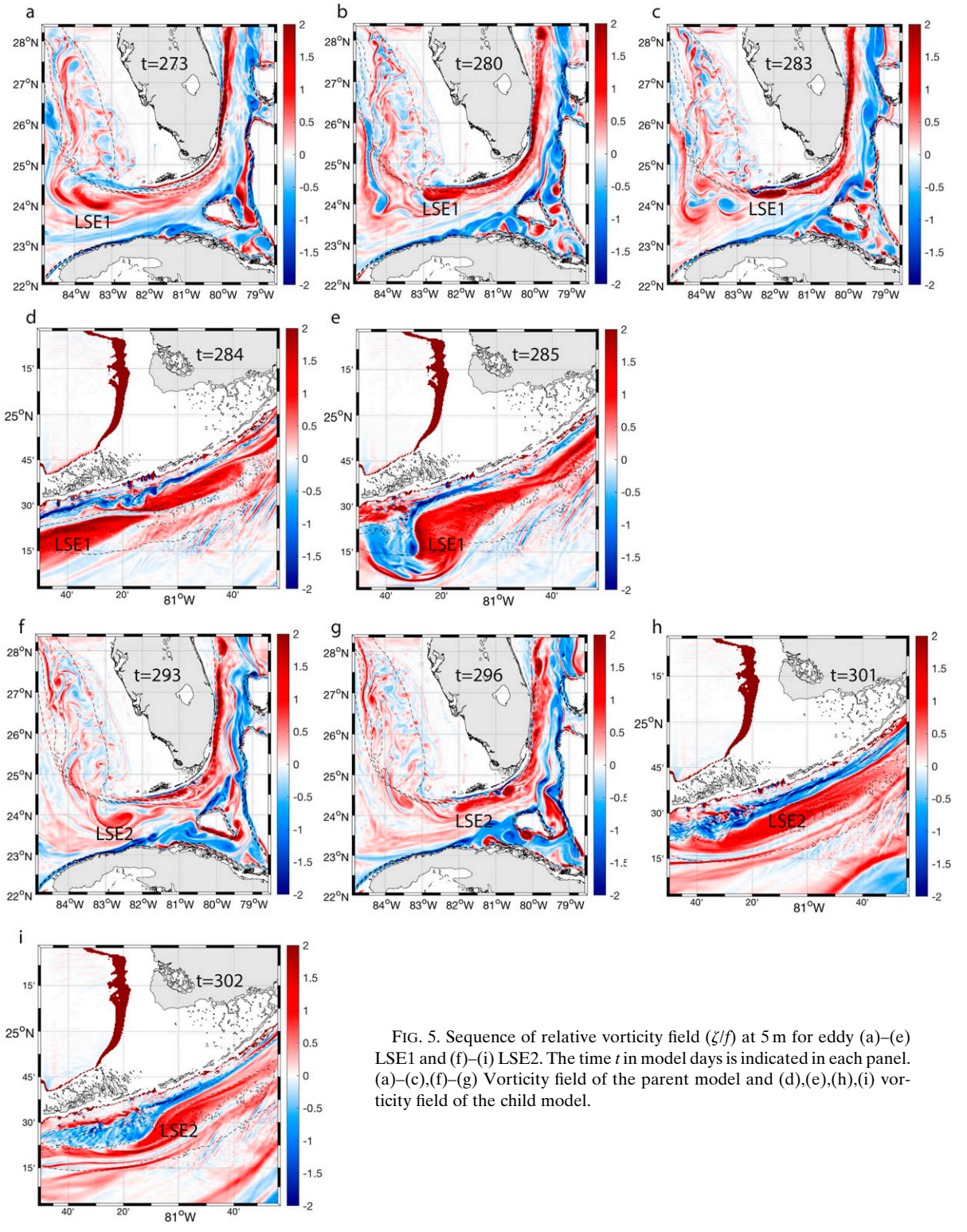

FIG. 5. Sequence of relative vorticity field (ζ/f) at 5 m for eddy (a)–(e) LSE1 and (f)–(i) LSE2. The time t in model days is indicated in each panel. (a)–(c),(f)–(g) Vorticity field of the parent model and (d),(e),(h),(i) vorticity field of the child model.

horizontal velocities in this frame of reference are u and v. For this analysis, the local mean, denoted by an overbar, is defined as the alongfront average for the region considered at a given time step. Perturbations relative to the mean are denoted with a prime such that all variable can be written $u = \overline{u} + u'$, where u is the absolute field. The mean kinetic to eddy kinetic energy conversion can be written as the sum of the horizontal shear production (HSP) and the vertical shear production (VSP):

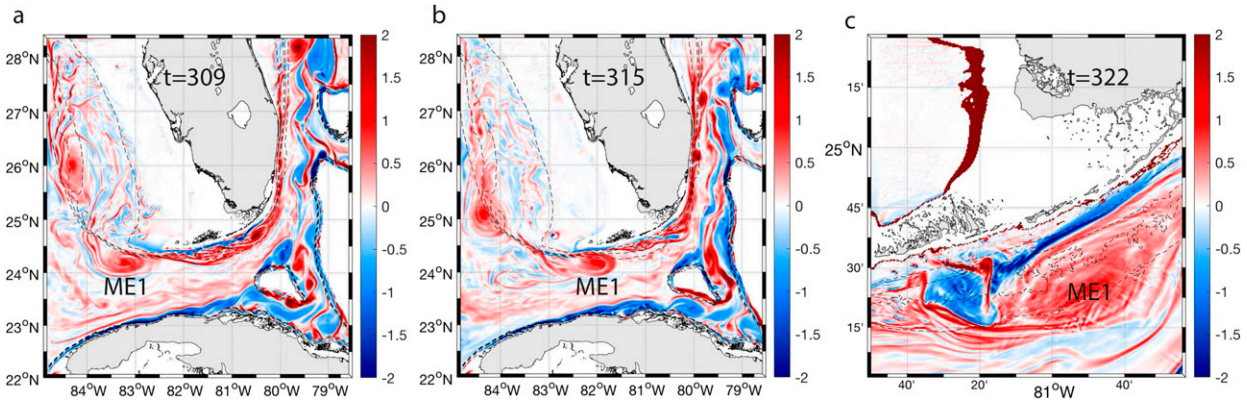

FIG. 6. Sequence of relative vorticity field (ζ/f) at 5 m for eddy ME1. The time t in model days is indicated in each panel. (a),(b) Vorticity field of the parent model and (c) vorticity field of the child model.

$$K_m K_e = \mathrm{HSP} + \mathrm{VSP}, \tag{1}$$

where

$$\mathrm{HSP} = -\overline{u'^2}\frac{\partial \overline{u}}{\partial x} - \overline{u'v'}\frac{\partial \overline{u}}{\partial y} - \overline{v'^2}\frac{\partial \overline{v}}{\partial y} - \overline{u'v'}\frac{\partial \overline{v}}{\partial x} \tag{2}$$

and

$$\mathrm{VSP} = -\overline{u'w'}\frac{\partial \overline{u}}{\partial z} - \overline{v'w'}\frac{\partial \overline{v}}{\partial z}. \tag{3}$$

The eddy potential to eddy kinetic energy conversion is the vertical eddy buoyancy flux (VBF)

$$P_e K_e = \overline{w'b'}, \tag{4}$$

where b is the buoyancy anomaly relative to the local area average. The instantaneous energy conversion terms were calculated for each one of the 11 cases listed in Table 1 except for the mesoscale eddy, which was not significantly affected by local instabilities in comparison to LSE1 and LSE2.

1) LOCALLY DESTABILIZED INCOMING EDDIES

The FB-ROMS nested model enables the occurrence of dynamical processes not usually observed in numerical simulations of this oceanic region. Indeed, studies of the Gulf Stream submesoscale dynamics, whether in the GS frontal eddies (Gula et al. 2016) or cold filaments (Gula et al. 2014) provided new insights on the dynamics of submesoscale instabilities in the subtropical region of the GS system. Incoming eddies, as previously identified are strongly elongated in the southern SoF and as such undergo a significant shear on their northern boundary that becomes unstable as shown by the perturbation seen in Fig. 5 and by the peak in HSP associated with the northern front the incoming eddies (Fig. 8). While barotropic instability dominates for LSE2, a peak in VBF is also seen for LSE1 on the northern front, which suggests that a mixed baroclinic–barotropic instability is developing. The latter formed a barotropic dipole in less than 24 h as shown in Fig. 5 unlike the barotropic instability alone.

2) LOCALLY FORMED SUBMESOSCALE EDDIES

Most submesoscale frontal eddies emanate from the growth of perturbations on superinertial vorticity filaments present near the top of the shelf slope in less than 200 m of water (Fig. 3). If the perturbations are sustained by the shear instability in that region of the FC, it is likely that the dominant instability is barotropic. Figure 9 confirms that the dominant mechanism is barotropic instability associated with a peak in

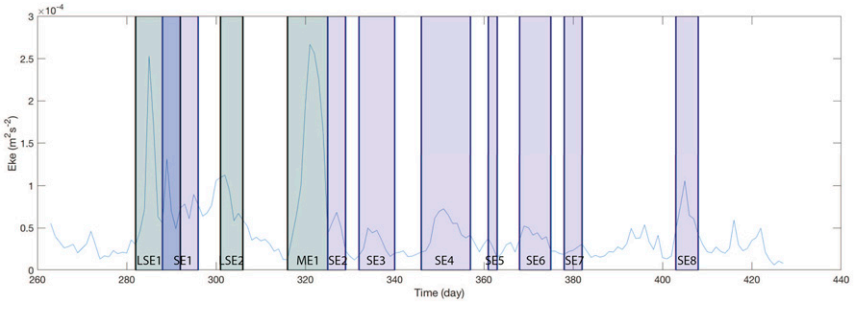

FIG. 7. Time series of the eddy kinetic energy (EKE) averaged along and across the cyclonic frontal region of the FC in the FB-ROMS grid. The shaded rectangles show the period of formation of all the frontal eddies identified in this study.

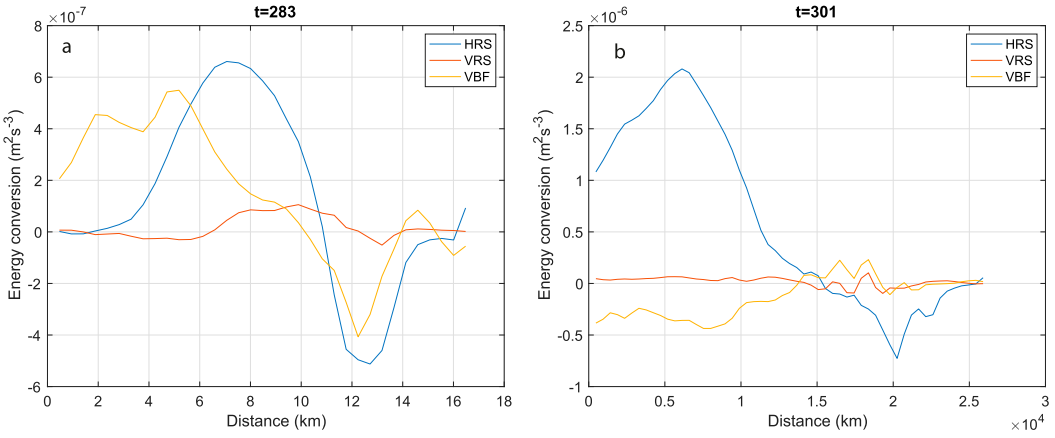

FIG. 8. Depth integrated and along shear front average HSP, VSP, and VBF across the frontal region north of (a) LSE1 and (b) LSE2 where the instabilities developed (Fig. 5). The time t in model days is indicated in each panel. The origin of the curves is on the southern side of the sheared region.

HSP with a few exceptions where VBF is the dominant energy transfer toward the perturbation (SE3), and where both VBF and HSP dominate the energy transfer (SE2, SE4, and SE7). In the case of SE3, two parallel vorticity filaments rolled up together to form the frontal eddy and this interaction was the product of a baroclinic instability. SE2 formation involved an anticyclonic counterpart which was sustained by a mixed baroclinic–barotropic instability. SE4 was dominated by barotropic instability on the south side of the shear zone although baroclinic instability developed on the shelf side of the shear zone. All the regimes that exhibited baroclinic instability were characterized by weakly stratified waters and weak shear near the shelf (Figs. 10b,c,d,g).

In all baroclinic cases Ertel's vorticity anomaly shows that Charney–Stern condition for baroclinic instability is met as the vorticity gradient changes sign vertically. The regimes that were sustained by barotropic instability only were characterized by a strong shear near the shelf (Figs. 10e,f) or a strongly stratified environment (Figs. 10a,h) in the upper part of the shelf slope, which prohibits the development of baroclinic instability despite favorable conditions for baroclinic instability for SE5 and SE6 (Figs. 10e,f) according to Charney–Stern criterion. The quasigeostrophic (QG) dynamics is formally invalid when Ro $\simeq$ 1, which can happen when the existing buoyancy gradient ∇b increases to large values. However, in the weakly stratified region this gradient is small and therefore the QG dynamics Charney Stern criterion applicable.

3) WEST FLORIDA SHELF WATER DRIVEN BAROCLINIC INSTABILITY

The analysis of the frontal instabilities in the simulation were conducted between model months October and February when weather patterns over the WFS contribute to significant cooling (He and Weisberg 2002). Cross sections in Fig. 10 show that WFS waters are characterized by negative PV values, spill over the shelf slope in the southern SoF, and therefore provide sustained conditions for the development of baroclinic instability when they interact with FC waters. It appears that those conditions are always present during the cold months but the growth of baroclinic instability is dictated by the absence of shear above the shelf, hence the growth of barotropic instability. Baroclinic instability would contribute to the mixing of waters of oppositely signed PV together, which would drive the PV toward zero, limiting the export of WFS waters across the FC. Nonetheless, nonlinear features associated with baroclinic instabilities expanded farther across the FC than nonlinear features formed by barotropic instability. Strongly stratified FC waters below the negative PV waters block the downslope spreading and hence the export. This situation differs from overflow dynamics in the Arctic region for instance where dense along slope jets become baroclinically unstable, which leads to rapid downslope eddy transport of dense water (Yankovsky and Legg 2019).

5. Bottom vorticity generation

Coastal vorticity filaments instability was shown to be associated with frontal shear instability dominated by barotropic instability. Vertical sections of the formed frontal eddies revealed the vertical extension of the eddy vorticity field, which hugged the bottom of the shelf slope (Fig. 3). Cross sections of the vorticity filaments before the eddy formation and near the tip of the FKRT reveal the sustained vorticity filaments extending from the bottom to the surface (Fig. 11). The bottom region underlying the vorticity filament is comprised between 50 and 170 m at 81°21.72′W in all cases. Downstream of our study region, Gula et al. (2015b) demonstrated that the bottom drag against the slope amplifies the cyclonic shear associated with vorticity filaments by generating large potential vorticity values within the slope turbulent bottom boundary layer (Molemaker et al. 2015).

To demonstrate this assumption and the fact that increased bottom vorticity flux is indeed associated with the formation of submesoscale eddies between the shelf slope of the FKRT and the cyclonic edge of the FC, we calculated the PV flux at the bottom as done in Gula et al. (2015b). We computed

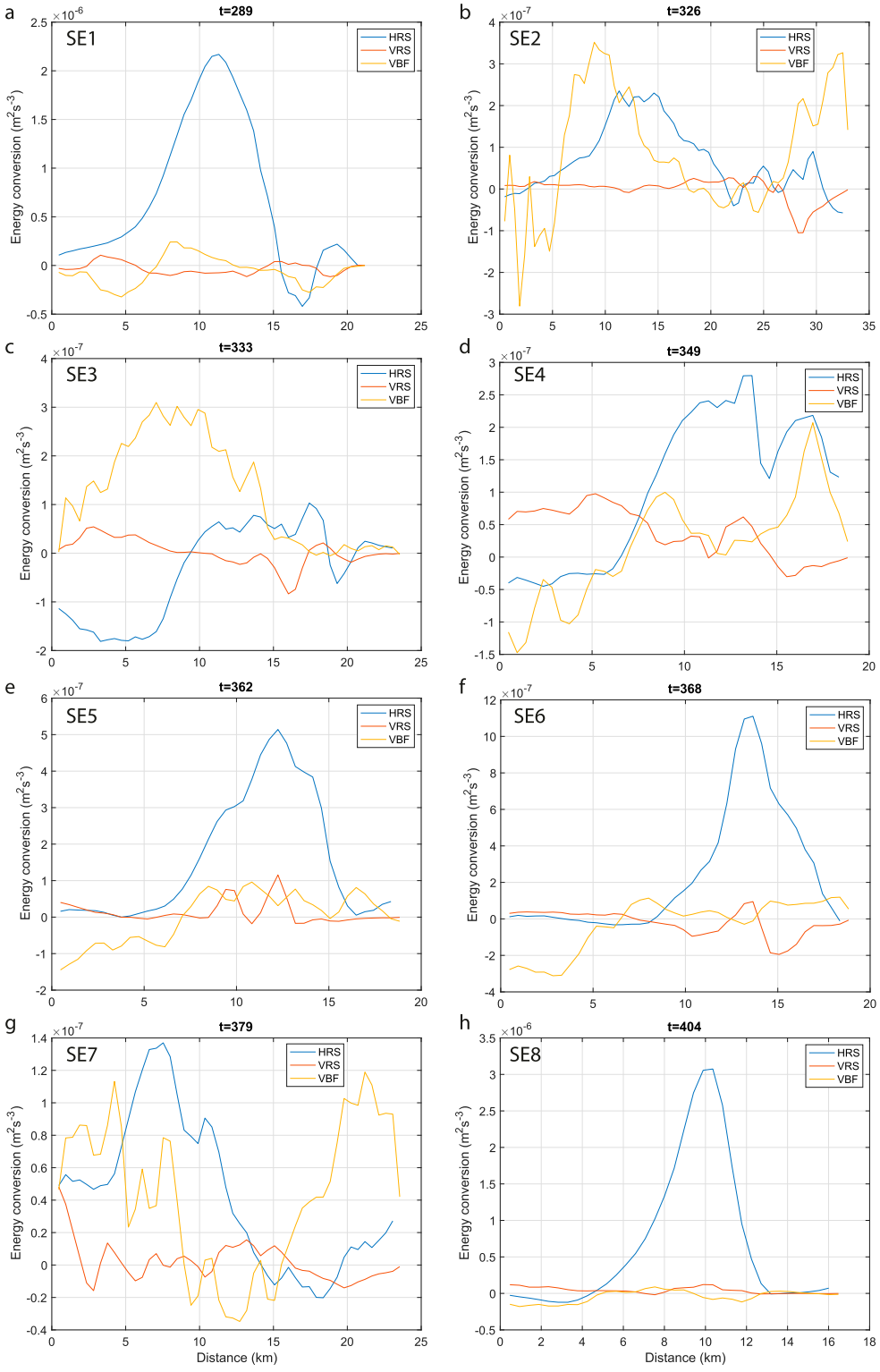

FIG. 9. As in Fig. 8, but for SE1–8.

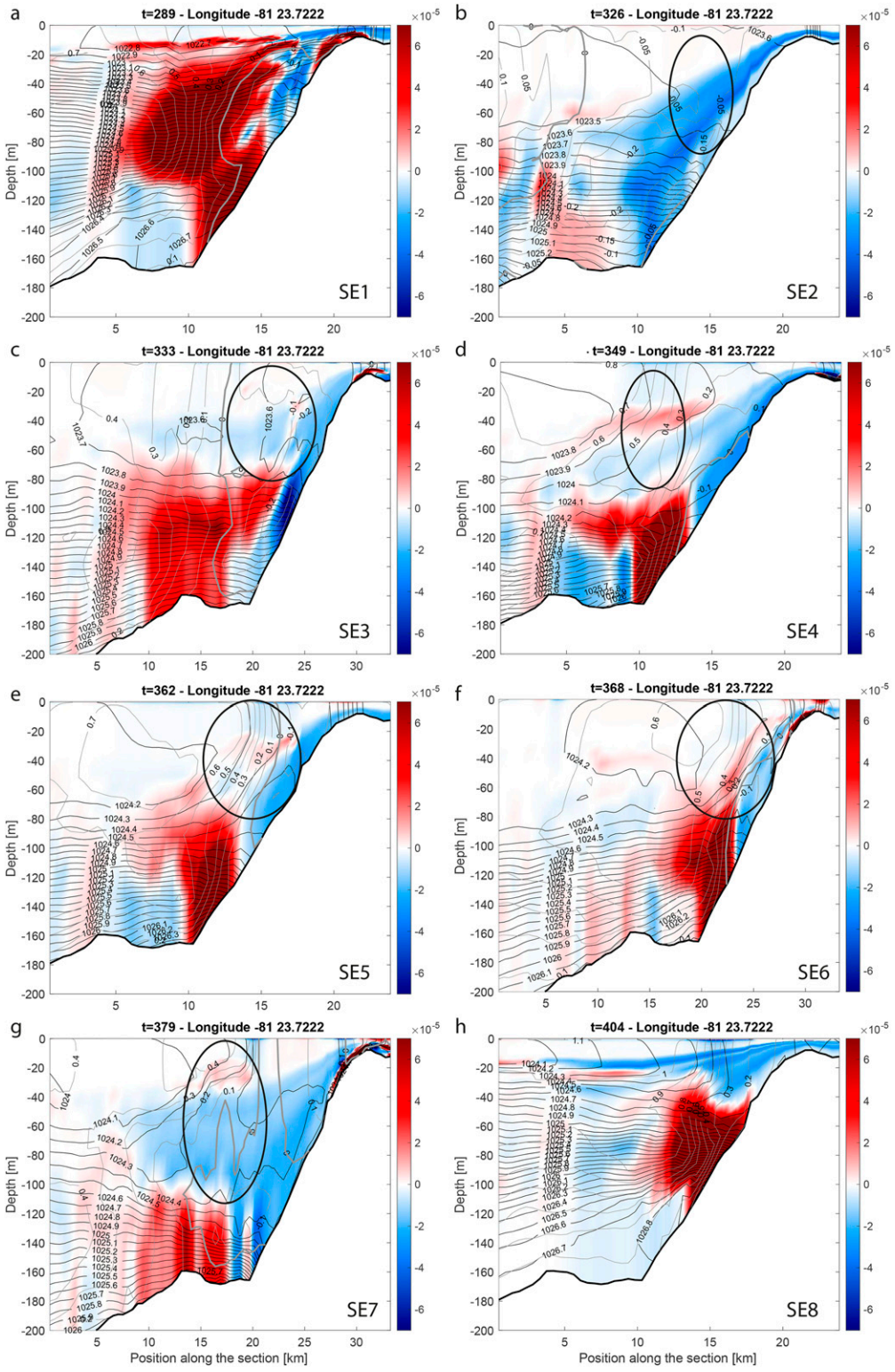

FIG. 10. Sequence of Ertel's vorticity anomaly (s^{-3}) cross sections at 81°23.7222′W 1 or 2 days prior to the formation of the submesoscale eddies (a) SE1, (b) SE2, (c) SE3, (d) SE4, (e) SE5, (f) SE6, (g) SE7, and (h) SE8. The time t in model days is indicated above each panel. Black contours show the density in kg m^{-3}. The density interval is 0.1 kg m^{-3}. Gray contours show the zonal velocity in m s^{-1}. Gray thick line shows the zero-velocity contour. The velocity interval is 0.05 m s^{-1}. The circled area shows the region were Ertel's vorticity anomaly changes sign vertically.

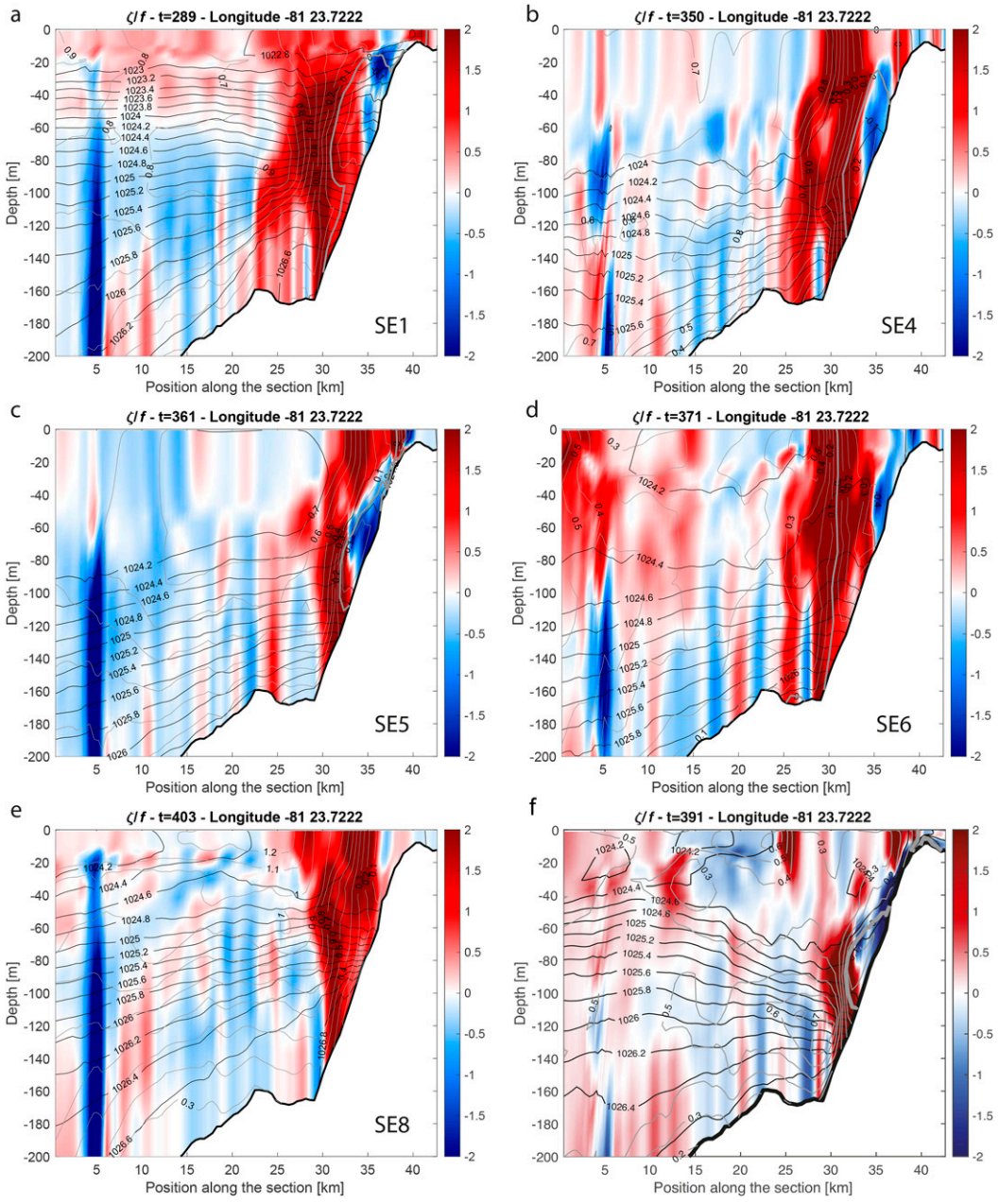

FIG. 11. Sequence of relative vorticity (ζ/f) cross sections at 81°23.7222′W 1 or 2 days prior to the formation of the submesoscale eddies (a) SE1, (b) SE4, (c) SE5, (d) SE6, and (e) SE8. (f) Relative vorticity during the period between SE7 and SE8 when vorticity filaments are broken by the southward shift of the Florida Current. The time t in model days is indicated above each panel. Black contours show the density in kg m^{-3}. The density interval is 0.2 kg m^{-3}. Gray contours show the zonal velocity in m s^{-1}. Gray thick line shows the zero velocity contour. The velocity interval is 0.1 m s^{-1}.

$\mathbf{J}_{\text{bot}} \cdot \mathbf{n} = \nabla_b \times \mathbf{F}_b \cdot \mathbf{n}$, where $\mathbf{n}$ is the unit vector normal to the bottom pointing into the water and $\mathbf{F}_b$ is the vertical gradient of stress at the bottom. In our simulation, the upward flux of horizontal momentum is approximated by $\mathbf{F}_b \approx r\mathbf{U}_b$, where $\mathbf{U}_b$ is the near bottom horizontal velocity and $r = 8 \times 10^{-4}$ m s^{-1}, the friction coefficient used in the linear bottom friction parameterization. The bottom PV flux was calculated over the entire model period analyzed in this study and the Hovmöller diagram of $\mathbf{J}_{\text{bot}} \cdot \mathbf{n}$ along a meridional section at 81°23.72′W is shown in Fig. 12. The top end of the section is located at the 50-m isobath and the bottom end is located 45 km south of it. The 150 m isobath is located about 4 km south of the 50 m isobath. Figure 12 reveals that all submesoscale eddy formations, by barotropic instability, were associated with a significant increase in bottom vorticity flux over the 50–180-m-isobath region that reached

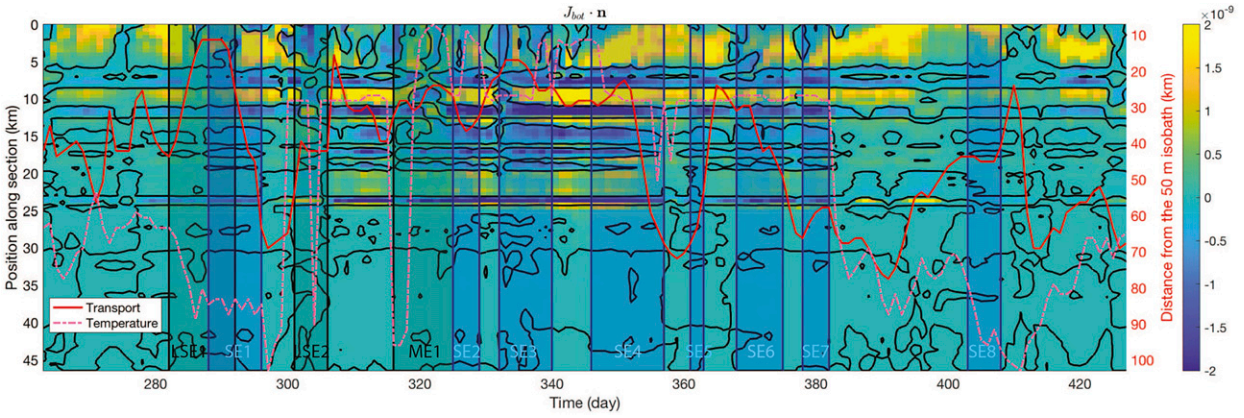

FIG. 12. Hovmöller diagram of the $\mathbf{J}_{\text{bot}} \cdot \mathbf{n}$ (m s^{-4}) along a meridional section at 81°23.72′W. The origin of the cross-shelf section is the 50-m isobath. The time is in model days. The red and solid (dashed and pink) line shows the distance from the 50-m isobath of the 12-Sv transport streamline (the 20°C isotherm at 150 m).

amplitudes higher than 10^{-09} m s^{-4}, higher than what was calculated in Gula et al. (2015b).

The 12 Sv (1 Sv $\equiv 10^6$ m^3 s^{-1}) transport streamline distance from the 50-m isobath in conjunction with the 20°C isotherm at 150 m (Lee et al. 1995; Kourafalou and Kang 2012) was used to estimate the distance of the FC front from the shelf slope. It appears that the position of the transport streamline is not always in phase with the 20°C isotherm at 150 m. In addition, none of these proxies for the location of the FC from the shelf slope appears to be correlated with the period of bottom vorticity intensification. However, the Ertel's PV anomaly cross sections in Fig. 10 shows that the FC highly sheared region varies vertically in depth as well. This observation also reveals that the area of contact with the shelf slope varies in depth and can be decoupled from the shallow unstratified region of the FC as seen in Fig. 10 for SE4, SE5, SE6, and SE8. The distance of the surface highly sheared region may not reflect the actual distance from the shelf of the same shear region at depth, as can be seen for SE4, SE5, and SE6 in Fig. 10. Conversely, the closeness of the 20°C isotherm at 150 m is not indicative of the presence of a highly sheared region near the shelf slope as seen for SE2 and SE3 in Fig. 12. The lateral and vertical oscillations of the baroclinic structure of the FC appear to be responsible for the depth of impingement of the highly sheared region of the FC on the shelf. These periods of impingement are associated with the generation of substantial bottom vorticity flux that contributes to the generation of superinertial vorticity filaments that quickly develop into a vortex street. A southern generation area can be observed in much deeper water. But it is associated with the rugged bottom bathymetry of the Pourtales Terrace south of the shelf slope along this section in depths greater than 200 m.

There is, however, a period between SE7 and SE8 during which the vorticity bottom flux is positive in the upper part of shelf (Fig. 12). This period is characterized by a significant offshore shift of the FC, which leaves behind remnants of the highly sheared region on the northern side of the current, which contains numerous vorticity filaments (Fig. 2, t = 391 days). When compared to the unstable filament regimes, a cross section of ζ shows that the FC southward shift, associated with WFS water overflow downwelling, breaks the vertical structure of the vorticity filaments, which become disconnected from the bottom PV flux (Fig. 11f, t = 391 days), hence stops short the instability development.

6. Summary and conclusions

This study provides a comprehensive overview and understanding of the SoF shelf slope dynamics based on a realistic high-resolution ROMS simulation of the South Florida oceanic region. To resolve the fine scale circulation, the simulation consisted of a two-way nested model in order to allow dynamic interactions across grids (Debreu et al. 2012). The nested simulation, with a 500-m resolution was analyzed to study the formation of the frontal eddies in the southern SoF. It is worth mentioning that the analysis was conducted over the model months October 2003 to February 2004, when the FC cyclonic edge was flowing over the shelf slope and submesoscale frontal eddies were present. Past this time period, the LC pushed the northern edge of the FC farther south, and the formation of frontal eddies stopped.

Although the model circulation was shown to be consistent with observations in a previous study (Criales et al. 2015), the eddies formed in the model were similar in size and shape to remotely observed eddies in the same area (Fig. 1). Two types of eddies are seen in Fig. 1 and their equivalent in the model are also shown. We now know that the smaller frontal eddies (Figs. 1a,b,d) are the product of barotropic instability, while the larger eddy in this sequence (Figs. 1c,f) is the product of baroclinic instability, at least in the model. Therefore, these observations provide substantial support to the dynamics simulated in the model. We used the model simulation to further study the dynamics and the nature of the instabilities that led to the formation of the frontal eddies in the SoF.

All but one eddies analyzed in this study were submesoscale as defined in Table 1. Two broad types of eddies were analyzed in this study:

1) Incoming LC frontal eddies that are strongly elongated by the FC strain, but whose northern front impinges on the shelf slope where it becomes unstable to mixed baroclinic–barotropic instability in the case of LSE1 and to barotropic instability only in the case of LSE2. The mixed instability nonlinear regimes was associated with the formation of a dipole that expanded farther across the FC than any other nonlinear regimes seen in this simulation. ME1, was the exception to the previous two. ME1 remained a mesoscale eddy although some filaments within the eddy exhibited values of $\zeta/f > 1$ locally. ME1 was not as elongated by the FC and therefore the shear on its northern side did not develop into an unstable wave (Fig. 6). The difference between the LSE and ME was due to the relative position of the FC to the northern shelf (Fig. 13). For LSE eddies, the FC was up against the shelf slope, with strong shear generated over the shelf slope. In the case of ME1 the same isopycnals were deeper by about 30 m, and the strong bottom friction sustained shear was absent.
2) Locally formed submesoscale eddies. They were mainly formed by barotropic instability in instances when the FC was strongly impinging on the northern shelf in the southern SoF. In situations where the FC shear region moved away from the shelf slope, baroclinic instability sustained by the overflow of negative PV WFS waters would develop and form submesoscale eddies, some of them being barotropic dipoles like SE2. The cross-stream penetration of the overflowing shelf waters is broken by the development of the frontal instabilities that limit their expansion across the strait. This effect significantly limits the export and the mixing of shelf waters with the FC waters. Shelf waters are mostly contained along the shelf slope in the SoF, until they reach the Gulf Stream region where more crossing can be observed. As a consequence, such limited cross-shelf dispersal would contribute to local retention of coral reef marine organisms that would be able to remain in the vicinity of a potential recruitment habitat. Conversely, toxic waters emanating from the shelf would remain longer in the vicinity of the FKRT coral reef ecosystem, adversely affecting the ecosystem's health.

Although not quantified in this study, the intermittence of the barotropic eddy formation is linked to the lateral "sloshing" of the FC as previously observed by Zantopp et al. (1987) at 27°N in the northern SoF. Fluctuations of current velocities and temperature in the 2–20-day frequency band is dominated by energy associated with FC meanders. Northward velocities at the shelf break decreased from about 1 m s^{-1} to near zero, with southward flow occurring on the onshore side of the front along the sloping bottom topography (see SE3 and SE7 in Fig. 10). Johns and Schott (1987) find that the most coherent, energetic meandering events occur at periods near 5 and 12 days. The passage of meanders leads to a sloshing of the thermocline, with upwelling and downwelling of isopycnals rearranging the cross stream structure of the current (Chester et al. 1991). Our model reveals that the FC meanders propagate through the southern SoF, with a probable origin in the GoM as shown by the similar period of the meanders observed around the LC by Donohue et al. (2016).

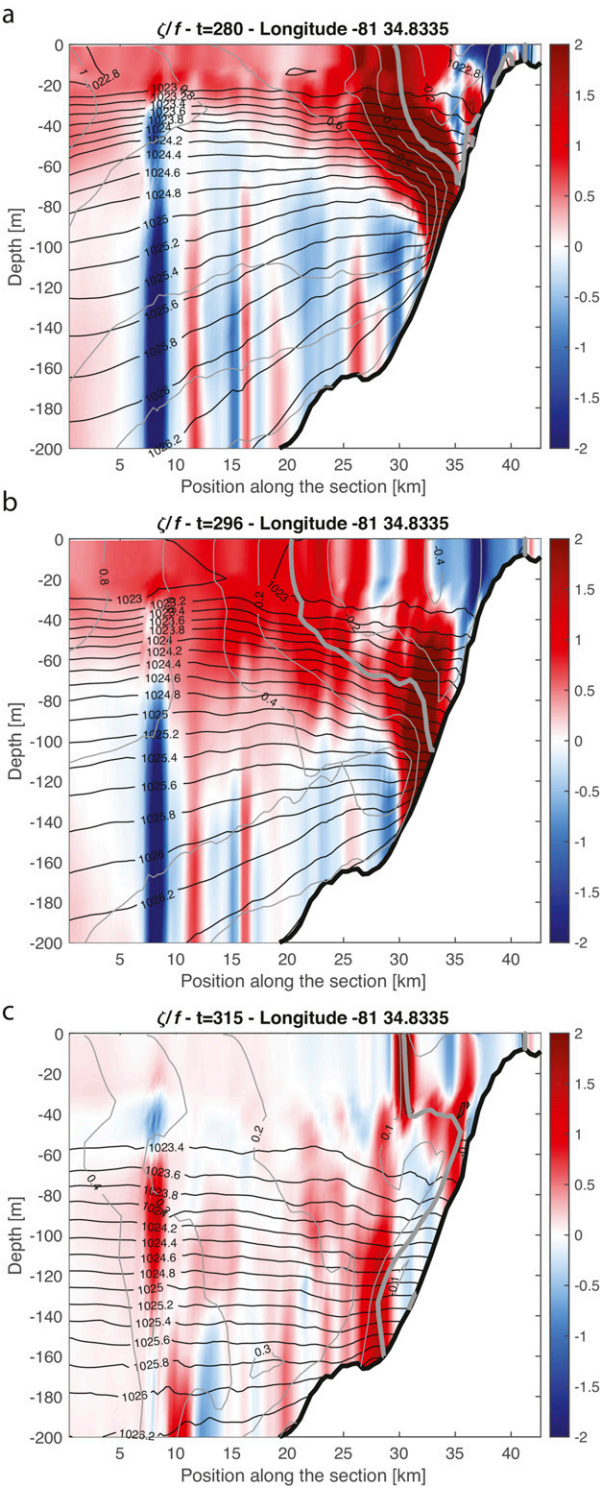

FIG. 13. Relative vorticity (ζ/f) cross sections at 81°34.8335′W showing the position of the Florida Current relative to the shelf slope before the passage of (a) LSE1, (b) LSE2, and (c) ME1.

All frontal eddies were formed from the breakup of vorticity filaments intensified by the injection of vorticity created by the friction of the FC on the shelf slope of the southern SoF. This mechanism was first proposed by Gula et al. (2015b) to explain the formation of frontal spinoff eddies in the northern SoF. Our results confirm the role of this mechanism and its ubiquity in the formation of the FC frontal eddies in the southern SoF. However, this process is subject to the location of the FC northern front according to the shelf slope. In regimes where the FC frontal region is pushed farther south, and away from the shelf slope, the formation of eddies by barotropic instability no longer happens but can be replaced by eddies formed by baroclinic instability due to the overflow of negative PVA WFS waters. Finally, instabilities start developing at the beginning of the FKRT, which is the region where the shelf slope expands farther below the FC, which introduces more frictional effects on the FC as well as on the shelf bottom circulation.

Acknowledgments. This study was supported in part by NOAA Grant Coastal and Ocean Climate Applications NA12OAR4310105 and by the Harbor Branch Oceanographic Institute Foundation. The authors are thankful to the anonymous reviewers for their thoughtful comments.

Data availability statement. ROMS simulation outputs are available upon request to the authors. The MODIS images were obtained from the Optical Oceanography Observatory at University of South Florida.

REFERENCES

Archer, M. R., L. K. Shay, B. Jaimes, and J. Martinez-Pedraja, 2015: Observing frontal instabilities of the Florida Current using high frequency radar. *Coastal Ocean Observing Systems*, Y. Liu et al., Eds., Elsevier, https://doi.org/10.1016/B978-0-12-802022-7.00011-0.

Barth, A., A. Alvera-Azcárate, and R. H. Weisberg, 2008: A nested model study of the Loop Current generated variability and its impact on the West Florida Shelf. *J. Geophys. Res.*, **113**, C05009, https://doi.org/10.1029/2007JC004492.

Beal, L. M., J. M. Hummon, E. Williams, O. B. Brown, W. Baringer, and E. J. Kearns, 2008: Five years of Florida current structure and transport from the Royal Caribbean Cruise Ship *Explorer of the Seas*. *J. Geophys. Res.*, **113**, C06001, https://doi.org/10.1029/2007JC004154.

Boccaletti, G., R. Ferrari, and B. Fox-Kemper, 2007: Mixed layer instabilities and restratification. *J. Phys. Oceanogr.*, **37**, 2228–2250, https://doi.org/10.1175/JPO3101.1.

Brooks, I. H., and P. P. Niiler, 1977: Energetics of the Florida Current. *J. Mar. Res.*, **35**, 163–191.

Capet, X., J. C. McWilliams, M. J. Molemaker, and A. F. Shchepetkin, 2008: Mesoscale to submesoscale transition in the California Current System. Part II: Frontal processes. *J. Phys. Oceanogr.*, **38**, 44–64, https://doi.org/10.1175/2007JPO3672.1.

Casey, K. S., T. B. Brandon, P. Cornillon, and R. Evans, 2010: The past, present, and future of the AVHRR pathfinder SST program. *Oceanography from Space*, V. Barale, J. Gower, and L. Alberotanza, Eds., Springer, 273–287, https://doi.org/10.1007/978-90-481-8681-5_16.

Chassignet, E. P., and Coauthors, 2009: U.S. GODAE: Global Ocean Prediction with the HYbrid Coordinate Ocean Model (HYCOM). *Oceanography*, **22**, 64–75, https://doi.org/10.5670/oceanog.2009.39.

Chester, D. B., P. Malanotte-Rizzoli, and H. DeFerrari, 1991: Acoustic tomography in the Straits of Florida. *J. Geophys. Res.*, **96**, 7023–7048, https://doi.org/10.1029/91JC00007.

Criales, M. M., L. M. Chérubin, and J. A. Browder, 2015: Modeling larval transport and settlement of the pink shrimp in south Florida: dynamics of behavior and tides. *Mar. Coast. Fish.*, **7**, 148–176, https://doi.org/10.1080/19425120.2014.1001541.

Davis, K. A., J. J. Leichter, J. L. Hench, and S. G. Monismith, 2008: Effects of western boundary current dynamics on the internal wave field of Southeast Florida shelf. *J. Geophys. Res.*, **113**, C09010, https://doi.org/10.1029/2007JC004699.

Debreu, L., P. Marchesiello, P. Penven, and G. Cambon, 2012: Two-way nesting in split-explicit ocean models: Algorithms, implementation and validation. *Ocean Modell.*, **49–50**, 1–21, https://doi.org/10.1016/j.ocemod.2012.03.003.

Donohue, K. A., D. Watts, P. Hamilton, R. Leben, M. Kennelly, and A. Lugo-Fernaìndez, 2016: Gulf of Mexico Loop Current path variability. *Dyn. Atmos. Oceans*, **76**, 174–194, https://doi.org/10.1016/j.dynatmoce.2015.12.003.

Egbert, G. D., and S. Y. Erofeeva, 2002: Efficient inverse modeling of barotropic ocean tides. *J. Atmos. Oceanic Technol.*, **19**, 183–204, https://doi.org/10.1175/1520-0426(2002)019<0183:EIMOBO>2.0.CO;2.

Evans, D. G., Frajka-Williams, E., Naveira Garabato, A. C., Polzin, K. L., and Forryan, A., 2020: Mesoscale eddy dissipation by a "zoo" of submesoscale processes at a western boundary. *J. Geophys. Res. Oceans*, **125**, e2020JC016246, https://doi.org/10.1029/2020JC016246.

Fiechter, J., and C. N. Mooers, 2003: Simulation of frontal eddies on the east Florida Shelf. *Geophys. Res. Lett.*, **30**, 2151, https://doi.org/10.1029/2003GL018307.

Fratantoni, P. S., T. N. Lee, G. Podesta, and F. Muller-Karger, 1998: The influence of Loop Current perturbations on the formation and evolution of Tortugas eddies in the southern Straits of Florida. *J. Geophys. Res.*, **103**, 24 759–24 779, https://doi.org/10.1029/98JC02147.

Gula, J., M. J. Molemaker, and J. C. McWilliams, 2014: Submesoscale cold filaments in the Gulf Stream. *J. Phys. Oceanogr.*, **44**, 2617–2643, https://doi.org/10.1175/JPO-D-14-0029.1.

——, ——, and ——, 2015a: Gulf Stream dynamics along the southeastern U.S. seaboard. *J. Phys. Oceanogr.*, **45**, 690–715, https://doi.org/10.1175/JPO-D-14-0154.1.

——, ——, and ——, 2015b: Topographic vorticity generation, submesoscale instability and vortex street formation in the Gulf Stream. *Geophys. Res. Lett.*, **42**, 4054–4062, https://doi.org/10.1002/2015GL063731.

——, J. M. Molemaker, and J. C. McWilliams, 2016: Submesoscale dynamics of a Gulf Stream frontal eddy in the South Atlantic Bight. *J. Phys. Oceanogr.*, **46**, 305–325, https://doi.org/10.1175/JPO-D-14-0258.1.

He, R., and R. H. Weisberg, 2002: West Florida shelf circulation and temperature budget for the 1999 spring transition. *Cont. Shelf Res.*, **22**, 719–748, https://doi.org/10.1016/S0278-4343(01)00085-1.

Johns, W. E., and F. Schott, 1987: Meandering and transport variations of the Florida Current. *J. Phys. Oceanogr.*, **17**, 1128–1147, https://doi.org/10.1175/1520-0485(1987)017<1128:MATVOT>2.0.CO;2.

Kalnay, E., and Coauthors, 1996: The NCEP/NCAR 40-Year Reanalysis Project. *Bull. Amer. Meteor. Soc.*, **77**, 437–472, https://doi.org/10.1175/1520-0477(1996)077<0437:TNYRP>2.0.CO;2.

Kourafalou, V. H., and H. Kang, 2012: Florida current meandering and evolution of cyclonic eddies along the Florida keys reef

tract: Are they inter-connected? *J. Geophys. Res.*, **117**, C05028, https://doi.org/10.1029/2011JC007383.

Krug, M., S. Swart, and J. Gula, 2017: Submesoscale cyclones in the Agulhas Current. *Geophys. Res. Lett.*, **44**, 346–354, https://doi.org/10.1002/2016GL071006.

Lapeyre, G., P. Klein, and B. L. Hua, 2006: Oceanic restratification forced by surface frontogenesis. *J. Phys. Oceanogr.*, **36**, 1577–1590, https://doi.org/10.1175/JPO2923.1.

Lee, T. N., 1975: Florida Current spin-off eddies. *Deep-Sea Res.*, **22**, 753–765.

——, 1986: Coastal circulation in the Key Largo Coral Reef Marine Sanctuary. *Physics of Shallow Estuaries and Bays*, J. van de Kreeke, Ed., Lecture Notes in Coastal and Estuarine Studies, Vol. 16, Springer, 178–198, https://doi.org/10.1029/LN016p0178.

——, and D. Mayer, 1977: Low-frequency current variability and spin-off eddies on the shelf off southeast Florida. *J. Mar. Res.*, **35**, 193–200.

——, and E. Williams, 1988: Wind-forced transport fluctuations of the Florida Current. *J. Phys. Oceanogr.*, **18**, 937–946, https://doi.org/10.1175/1520-0485(1988)018<0937:WFTFOT>2.0.CO;2.

——, J. A. Yoder, and L. P. Atkinson, 1991: Gulf Stream frontal eddy influence on productivity of the southeast U.S. continental shelf. *J. Geophys. Res.*, **96**, 22 191–22 205, https://doi.org/10.1029/91JC02450.

——, C. Rooth, E. Williams, M. McGowan, A. F. Szmant, and M. E. Clarke, 1992: Influence of Florida Current, gyres and wind-driven circulation on transport of larvae and recruitment in the Florida keys coral reefs. *Cont. Shelf Res.*, **12**, 971–1002, https://doi.org/10.1016/0278-4343(92)90055-O.

——, K. Leaman, E. Williams, T. Berger, and L. Atkinson, 1995: Florida Current meanders and gyre formation in the southern Straits of Florida. *J. Geophys. Res.*, **100**, 8607–8620, https://doi.org/10.1029/94JC02795.

Magaldi, M. G., T. M. Özgökmen, A. Griffa, E. P. Chassignet, M. Iskandarani, and H. Peters, 2008: Turbulent flow regimes behind a coastal cape in a stratified and rotating environment. *Ocean Modell.*, **25**, 65–82, https://doi.org/10.1016/j.ocemod.2008.06.006.

Manucharyan, G. E., and M. L. Timmermans, 2013: Generation and separation of mesoscale eddies from surface ocean fronts. *J. Phys. Oceanogr.*, **43**, 2545–2562, https://doi.org/10.1175/JPO-D-13-094.1.

Marchesiello, P., X. Capet, C. Menkes, and S. C. Kennan, 2011: Submesoscale dynamics in tropical instability waves. *Ocean Modell.*, **39**, 31–46, https://doi.org/10.1016/j.ocemod.2011.04.011.

McWilliams, J. C., 2016: Submesoscale currents in the ocean. *Proc. Roy. Soc.*, **472A**, 20160117, https://doi.org/10.1098/rspa.2016.0117.

Mesinger, F., and Coauthors, 2006: North American Regional Reanalysis. *Bull. Amer. Meteor. Soc.*, **87**, 343–360, https://doi.org/10.1175/BAMS-87-3-343.

Molemaker, M., J. McWilliams, and W. Dewar, 2015: Submesoscale instability and generation of mesoscale anticyclones near a separation of the California Undercurrent. *J. Phys. Oceanogr.*, **45**, 613–629, https://doi.org/10.1175/JPO-D-13-0225.1.

Molinari, R., and K. Leaman, 1987: Surface currents in the Straits of Florida. *Mar. Wea. Log*, **31**, 11–13.

Morvan, M., and X. Carton, 2020: Sub-mesoscale frontal instabilities in the Omani Coastal Current. *Mathematics*, **8**, 562, https://doi.org/10.3390/math8040562.

Peters, H., L. K. Shay, A. J. Mariano, and T. M. Cook, 2002: Current variability on a narrow shelf with large ambient vorticity. *J. Geophys. Res.*, **107**, 3087, https://doi.org/10.1029/2001JC000813.

Rayleigh, L., 1880: On the stability, or instability of certain fluid motions. *Proc. Roy. Soc. London*, **9**, 57–70.

Richardson, D. E., J. K. Llopiz, K. D. Leaman, P. S. Vertes, F. E. Muller-Karger, and R. K. Cowen, 2009: Sailfish (*Istiophorus platypterus*) spawning and larval environment in a Florida Current frontal eddy. *Prog. Oceanogr.*, **82**, 252–264, https://doi.org/10.1016/j.pocean.2009.07.003.

Shay, L. K., T. N. Lee, E. J. Williams, H. C. Graber, and C. G. H. Rooth, 1998: Effects of low frequency current variability on near-inertial submesoscale vortices. *J. Geophys. Res.*, **103**, 18 691–18 714, https://doi.org/10.1029/98JC01007.

——, and Coauthors, 2000: VHF radar detects oceanic submesoscale vortex along Florida coast. *Eos, Trans. Amer. Geophys. Union*, **81**, 209–213, https://doi.org/10.1029/00EO00143.

——, T. M. Cook, H. Peters, A. J. Mariano, R. H. Weisberg, P. E. An, A. Soloviev, and M. Luther, 2002: Very high-frequency radar mapping of surface currents. *IEEE J. Oceanic Eng.*, **27**, 155–169, https://doi.org/10.1109/JOE.2002.1002470.

——, J. Martinez-Pedraja, T. M. Cook, B. K. Haus, and R. Weisberg, 2007: High-frequency radar mapping of surface currents using WERA. *J. Atmos. Oceanic Technol.*, **24**, 484–503, https://doi.org/10.1175/JTECH1985.1.

Sponaugle, S., T. Lee, V. Kourafalou, and D. Pinkard, 2005: Florida Current frontal eddies and the settlement of coral reef fishes. *Limnol. Oceanogr.*, **50**, 1033–1048, https://doi.org/10.4319/lo.2005.50.4.1033.

Tedesco, P., J. Gula, C. Ménesguen, P. Penven, and M. J. Krug, 2019: Generation of submesoscale frontal eddies in the Agulhas Current. *J. Geophys. Res. Oceans*, **124**, 7606–7625, https://doi.org/10.1029/2019JC015229.

Yankovsky, E., and S. Legg, 2019: Symmetric and baroclinic instability in dense shelf overflows. *J. Phys. Oceanogr.*, **49**, 39–61, https://doi.org/10.1175/JPO-D-18-0072.1.

Zamudio, L., and P. J. Hogan, 2008: Nesting the Gulf of Mexico in Atlantic HYCOM: Oceanographic processes generated by Hurricane Ivan. *Ocean Modell.*, **21**, 106–125, https://doi.org/10.1016/j.ocemod.2007.12.002.

Zantopp, R. J., K. D. Leaman, and T. N. Lee, 1987: Florida Current meanders: A close look in June–July 1984. *J. Phys. Oceanogr.*, **17**, 584–595, https://doi.org/10.1175/1520-0485(1987)017<0584:FCMACL>2.0.CO;2.

Zhang, Y., C. Hu, Y. Liu, R. H. Weisberg, and V. H. Kourafalou, 2019: Submesoscale and mesoscale eddies in the Florida Straits: Observations from satellite ocean color measurements. *Geophys. Res. Lett.*, **46**, 13 262–13 270, https://doi.org/10.1029/2019GL083999.

Zhong, Y., and A. Bracco, 2013: Submesoscale impacts on horizontal and vertical transport in the Gulf of Mexico. *J. Geophys. Res. Oceans*, **118**, 5651–5668, https://doi.org/10.1002/jgrc.20402.